*sustainability*

MDPI

*Article*

# Design, Modelling and Optimization of a Novel Concentrated Solar Powered (CSP) Flash Desalination System Involving Direct Heating and Pressure Modulation Using Response Surface Methodology (RSM)

**Faizan Ahmed [1,2], Mohd Sharizal Abdul Aziz [1,*], Mohd Remy Rozainy Mohd Arif Zainol [3,*], Khor Chu Yee [4], Feroz Shaik [2], Dewi Suriyani Che Halin [5], Mohd Arif Anuar Mohd Salleh [5] and Marwan Kheimi [6]**

1 School of Mechanical Engineering, Engineering Campus, Universiti Sains Malaysia, Nibong Tebal 14300, Seberang Perai Selatan, Penang, Malaysia
2 Department of Mechanical Engineering, Prince Mohammad Bin Fahd University, Al Khobar 31952, Saudi Arabia
3 School of Civil Engineering, Engineering Campus, Universiti Sains Malaysia, Nibong Tebal 14300, Seberang Perai Selatan, Penang, Malaysia
4 Faculty of Mechanical Engineering & Technology, Universiti Malaysia Perlis (UniMAP), Arau 02600, Perlis, Malaysia
5 Faculty of Chemical Engineering Technology, Universiti Malaysia Perlis (UniMAP), Arau 02600, Perlis, Malaysia
6 Department of Civil Engineering, Faculty of Engineering-Rabigh Branch, King Abdulaziz University, Jeddah 21589, Saudi Arabia
* Correspondence: msharizal@usm.my (M.S.A.A.); ceremy@usm.my (M.R.R.M.A.Z.)

check for updates

**Citation:** Ahmed, F.; Abdul Aziz, M.S.; Mohd Arif Zainol, M.R.R.; Yee, K.C.; Shaik, F.; Che Halin, D.S.; Mohd Salleh, M.A.A.; Kheimi, M. Design, Modelling and Optimization of a Novel Concentrated Solar Powered (CSP) Flash Desalination System Involving Direct Heating and Pressure Modulation Using Response Surface Methodology (RSM). *Sustainability* **2022**, *14*, 11558. https://doi.org/10.3390/su141811558

Academic Editor: Ramchandra Pode

Received: 26 July 2022
Accepted: 8 September 2022
Published: 15 September 2022

**Publisher's Note:** MDPI stays neutral with regard to jurisdictional claims in published maps and institutional affiliations.



**Abstract:** The main problem with existing desalination technologies is that they consume high input energy to generate fresh water. Secondly, this energy demand is usually met by conventional sources of energy such as fossil fuels. With limited conventional energy reserves predicted for the future, the focus is on the utilization of renewable sources of energy such as solar, wind, and geothermal energy for powering desalination systems. Such a transformation would make the desalination systems more energy efficient, sustainable, and economical. In this paper, a novel concentrated solar powered (CSP) flash desalination system with direct heating and pressure modulation is presented. A lab-scale prototype was designed, manufactured, and tested for feed water collected from the Arabian Sea and in climatic conditions of Al-Khobar city in Saudi Arabia. The effect of three process parameters, namely, feed water temperature (30–40 °C), feed water flow rate (0.003–0.006 kg/s), and vacuum pressure (0.1–0.3 bar) on distillate production, was investigated. System modelling and optimization were done using Design Expert software and Response Surface Methodology (RSM). The central composite design technique was employed for the optimization of process parameters. The adequacy of the developed distillate production model was verified by ANOVA. The optimum values of feed water temperature, flow rate, and vacuum pressure are reported to be 40 °C, 0.005 kg/s, and 0.1 bar, respectively, resulting in distillate production of 0.001 kg/s.

**Keywords:** concentrated solar power; single stage; flash desalination; response surface methodology; optimization

## 1. Introduction

Solar desalination systems based on the flashing technique operate on the principle of quick vaporization resulting from the condition when a liquid is brought under its saturation pressure [1]. These systems have been extensively utilized for desalination due to their high evaporation rates [2]. They have also been used for other applications related to refrigeration [3] and dehumidification [4]. As such, these systems involve the use of the non-renewable source of energy for their operation. Hence, researchers' focus has shifted

towards integrating renewable energy sources such as solar energy in these systems [5,6]. However, some problems are associated with using solar energy for these systems. These issues include low radiation conditions and intermittent supply of radiation which affects the evaporation rate and subsequently the system's output. This leads to difficulties in practically implementing these renewable energy-based systems [7].

One approach to overcome such issues is combining the system with a thermal energy storage facility. To this extent, Miyatake et al. [8] investigated the performance of a flash evaporation system integrated with a latent heat storage facility. They reported an enhancement in efficiency by 95% for the system with a thermal heat storage feature. Similarly, Lai et al. [9] experimented with a reverse osmosis system based on solar energy with a thermal energy storage feature. They tested the setup for moderate working conditions and concluded that the system's efficiency augments by 9%. Another design configuration was explored by Ghorbani et al. [10]. They tested a multi-stage flashing system integrated with a solar collector. Further, a phase change material was also employed for thermal energy storage. It was reported that the phase change material could substantially enhance the heat storage capability of the system.

Another approach to enhancing the system performance when operated with non-renewable energy sources is by improving the design of the flash vaporization segments. In this aspect, the scholars are focusing on improvements in heat transfer and designing simple systems such as single-stage flash evaporation systems. For example, Gao et al. [11] investigated the performance of a flashing system using a visualization unit. They studied the effect of vacuum on the boiling characteristics inside a water droplet. Another study was conducted by Ji et al. [12], wherein the spray flashing was done at high pressure and high temperature. They concluded that the flashing condition significantly affects the bubble formation process and its growth. In another study, Muthunayagam et al. [13] investigated the temperature changes of water droplets during and after the spraying and developed a vapor model. From these studies, it can be interpreted that the main factors affecting the spraying process and the system performance are heat flux, operating pressure, and superheat temperature of the spray liquid. Furthermore, optimizing the design and operation of such a system is also essential for enhanced performance.

To this extent, Ikegami et al. [14] reported that an upward jet produces higher efficiency than a downward jet due to an increase in the water droplet flash path. However, in another study [15], it was reported that irrespective of whether the water jet flow is in the upward or downward stream, the system's efficiency increases with an increase in flow rate. However, at the same time, a decrease in flash efficiency was also observed.

The recent focus by many scholars has been on the utilization of nanoparticles in spray liquid. The main aim of suspending nanoparticles in spraying liquid is to increase the heat and mass transfer capabilities of the working fluid. Peng et al. [16] carried out an experimental investigation with $Al_2O_3$ nanofluid. The system's flash efficiency was enhanced due to the higher heat transfer capability of $Al_2O_3$ nanofluid. In another study, Guo et al. [17] numerically investigated the idea of micro encapsulating the water droplet with phase change material. It was reported that the microencapsulated water droplet significantly increased the evaporation rate. Numerous research studies were performed on this microencapsulation concept [18–20], and it was observed that the microencapsulated water droplet had higher thermal energy transfer. The use of the microencapsulated phase change material also resulted in performance improvement, as reported by Chen et al. [21]. In recent studies by Moharram et al. [22] and Gnaifaid et al. [23], the concept of simultaneous desalination and power generation using concentrated solar power was explored. The concentrated solar power technique was reported to be the future research direction.

In the previous studies, it has been observed that the enhancement in spray-type solar desalination systems is mainly by adding a thermal energy storage facility and improvement in the design of the flash chamber. Some studies also report the utilization of nanofluids, phase change material, and microencapsulation of water droplets for efficiency augmentation. However, in cases where the solar energy supply is intermittent

or inadequate, the temperature of the spraying liquid is dropped, resulting in a drop in system performance. Hence, this paper proposes a novel concentrating solar power-based flash desalination system with direct heating and pressure modulation. The effect of process parameters such as feed water temperature, flow rate, and vacuum pressure was investigated experimentally. Further, system modelling and optimization were done by Response Surface Methodology using Design Expert software. Figure 1 presents a schematic representation of modelling and optimization patterns for distillate production.

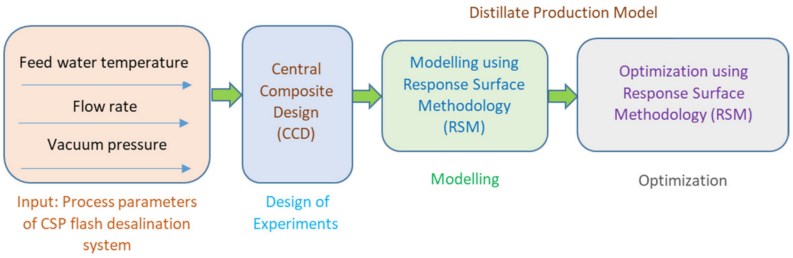


**Figure 1.** Schematic illustration of design, modelling, and optimization paradigm of the proposed system.

## 2. Experiments

### *2.1. Materials and Method*

The front view of the experimental apparatus is shown in Figure 2, whereas Figure 3 shows the back side view of the setup. Figure 4 presents the schematic of the apparatus along with the process flow directions. As seen in these figures, the main components of the setup include a feed water tank, pump with variable frequency drive, rotameter, pressure gauges, condenser, heat exchanger, concentrator plate, temperature sensors, flash chamber, nozzle, brine disposal tank, distillate tank, vacuum pump, and parabolic dish. The dimensions of these components are listed in Table 1. The material used for the base board was wood, whereas stainless steel was used for the condenser, heat exchanger, flash chamber, and connecting pipes. The feed water tank, brine disposal tank, and distillate collection tank were made of glass. The parabolic dish was of steel with an inner surface fitted with reflective mirrors to reflect solar radiation. Although the experimental runs were carried out with the most care, some uncertainty in measurements resulting from the measuring tools always exists. The various tools used for measurement, along with their range and uncertainties, are listed in Table 2.

**Table 1.** Components and their dimensions.

| S. No | Component | Dimensions/Specifications (L = Length, B = Breadth, H = Height) |
|---|---|---|
| 1 | Base board | 1.5 × 0.5 × 1.5 m (L × B × H) |
| 2 | Heat exchanger | 0.05 × 0.05 × 0.1 m (L × B × H) |
| 3 | Flash chamber | 0.1 × 0.1 × 0.2 m (L × B × H) |
| 4 | Condenser | 0.05 × 0.05 × 0.10 m (L × B × H) |
| colo5 | Pipes | 0.006 m |
| 6 | Nozzle | 0.002 m |
| 7 | Water tanks | 0.005 $m^3$ |
| 8 | Water pump | 368 W |
| 9 | Parabolic dish | Radius = 0.28 m, depth = 0.04 m |
| 10 | Copper plate | Diameter = 0.05 m |

**Table 2.** Measuring tools and their uncertainty.

| S. No | Parameter | Instrument | Range | Uncertainty |
|---|---|---|---|---|
| 1 | Flow rate | Rotameter | 0.003 to 0.06 kg/s | ±1.25% |
| 2 | Temperature | Type-K thermocouple | −50 to 1000 °C | ±1.25% |

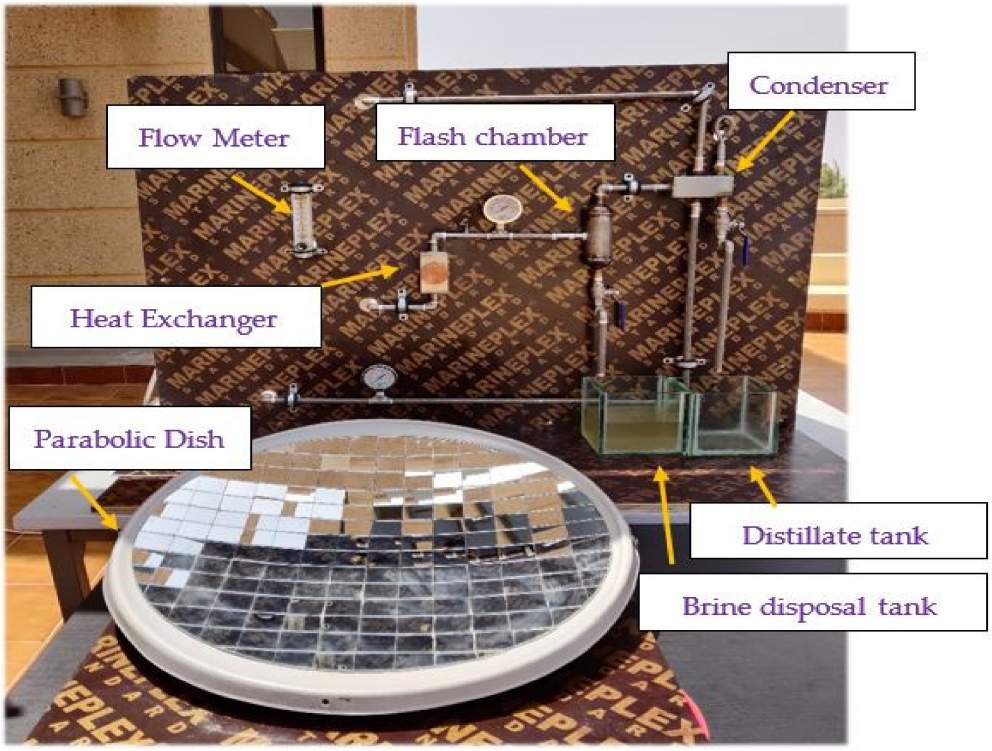


**Figure 2.** Front view of experimental apparatus.

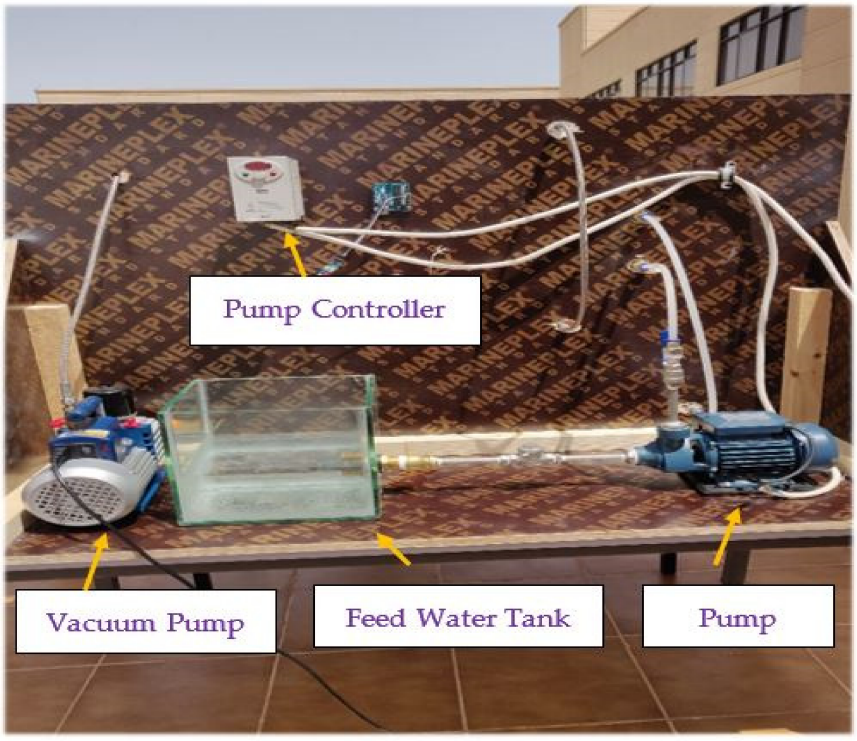


**Figure 3.** Back view of experimental apparatus.

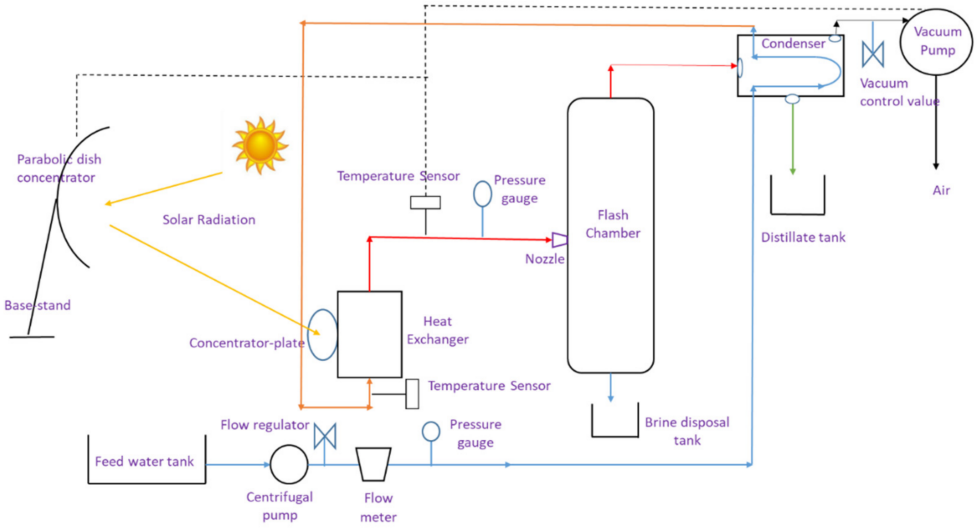


**Figure 4.** Schematic of the experimental setup.

Feed water was collected from the coastal sea of Al Khobar city in the eastern province of Saudi Arabia. It was then loaded into the feed water tank of the experimental setup. Each experiment was carried out for one hour to measure the distillate output per hour. The pump moves the feed water through the condenser coil and into the heat exchanger. The water picks up the heat while moving through the condenser coil and enters the heat exchanger. A copper plate is attached to the wall of this heat exchanger. In addition, a parabolic dish is used to reflect and concentrate the solar radiation onto this copper plate. As the feed water moves into and through this heat exchanger, it gets further heated due to the concentrated radiation falling on the heat exchanger wall. The heated feed water is then sprayed into a flash chamber utilizing a nozzle. The vapors generated in the flashing chamber are forced to move towards the condenser by applying vacuum pressure in the condenser. The vapors are then condensed onto the condenser coil and are collected separately in the distillate tank as the output. Brine solution accumulated at the bottom of the flash chamber is also collected in a separate brine collection tank.

### *2.2. Experiment Design Using RSM*

The Response Surface Methodology approach has been preferred and utilized by many scientists [24–28] to optimise various systems. Hence, in this study, Response Surface Methodology was utilized for designing the experiments and developing a model to evaluate the influence of three independent process parameters (A: feed water temperature, B: flow rate, C: vacuum pressure) on the response (R: distillate). These three process parameters can significantly affect the output of the system. They can influence the heating and cooling processes in the boiler and the condenser heat exchanger, ultimately affecting the system's output. Hence, they are chosen for this study. Additionally, the main objective of this experimental setup is to obtain distilled water. Hence, the amount of distillate collected is chosen as the response. A central composite design (CCD) technique was employed. This technique was based on eight factorial points, six axial points, and six replicate points at the center. The process parameters were varied at three levels (−1, 0, 1). The number of experimental tests was calculated using Equation (1).

$$N = 2^K + 2K + C \quad (1)$$

where $N$ is the experimental trials to be conducted, $K$ is the number of independent variables to be examined, and $C$ is the number of tests to be done for the central points. The limits for each factor are shown in Table 3. The limits for these parameters are chosen based on experimental capability and existing weather conditions. For example, the vacuum pump could provide the above ranges of vacuum pressure. Similarly, for most of the year in this

region, the average ambient temperature is in the range of 30–40 °C. Hence, the feed water temperature is tested for this condition. The matrix for experimental data was determined using Design Expert software version 13.0.5, Statease, Minneapolis. The subsequent model obtained was analyzed using ANOVA.

**Table 3.** Independent variables and their range with coded levels.

| Independent Variable | Coded Levels (Range) | | |
|---|---|---|---|
| | **−1** | **0** | **+1** |
| Flow rate (kg/s) | 0.003 | 0.0045 | 0.006 |
| Feed water temperature (°C) | 30 | 35 | 40 |
| Vacuum pressure (Pa) | 0.1 | 0.2 | 0.3 |

## 3. Results and Discussion

### *3.1. Model Development for Distillate Production*

Response Surface Methodology was used to investigate the interactivity of three parameters, namely, feed water temperature, flow rate, and vacuum pressure on distillate production. The design of the experiments and obtained responses are shown in Table 4. A maximum response of 0.001 kg/s was obtained at a feed water temperature of 40 °C, a flow rate of 0.005 kg/s, and a vacuum pressure of 0.1 bar. Likewise, a minimum response of 0.0004 kg/s was obtained at a feed water temperature of 30 °C, a flow rate of 0.003 kg/s, and a vacuum pressure of 0.3 bar. The results show that an increase in vacuum pressure resulted in a decrease in distillate production. Vacuum pressure across the condenser enables the movement of vapors from the flash chamber into the condenser. However, some vapor molecules are thrown out into the atmosphere with higher vacuum pressures even before being condensed. This situation results in a drop in distillate production. This behavior is synchronous with Mohammadi et al. [29], where the distillate production decreases with an increase in vacuum pressure. The following model (Equation (2)) in terms of coded levels is developed based on the results obtained:

$$Distillate = 3010 + 550A + 240B - 210C + 62.5AB + 62.5AC - 450B^2 \quad (2)$$

where in A, B, and C are coded values for three selected parameters, namely, feed water temperature, flow rate, and vacuum pressure, respectively. The ANOVA for the polynomial equation and the corresponding regression coefficients for distillate production is listed in Table 5. The significance of the developed model can be established from the F-value, *p*-value, correlation of determination ($R^2$) value, and results from the lack of fit test. The model was identified to be significant as the model F-value is 150.84. A specific model term is insignificant if that factor has a *p*-value greater than 0.05. In the present analysis, the significant model terms are identified as A, B, C, AB, AC, and $B^2$. The model terms are considered insignificant for *p*-values higher than 0.05. The F-value of 0.75 for the lack of fit test means that this lack of fit is non-significant compared to the pure error. It is preferred to have non-significance in lack of fit as this will lead to a good fit of the model. The predicted $R^2$ value of 0.96 agrees with the adjusted $R^2$ value of 0.97. The ratio of standard deviation to mean is referred to as the Coefficient of Variance (CV). The obtained CV value is 2.7%. A model is considered reproducible if the CV value is less than 10. The signal-to-noise ratio is called Adequate Precision (AP). It is desirable to have an AP ratio bigger than 4. In this analysis, an AP ratio of 44.95 was attained, indicating an adequate signal; hence, the model can be utilized for navigation of design space.

**Table 4.** Experiment design for distillate production.

| Run | Independent Variables | | | Responses | CCD Position |
|---|---|---|---|---|---|
| | Feed-Water Temperature, A | Flow Rate, B | Vacuum Pressure, C | Distillate Production kg/s | |
| 1 | 35 | 0.006 | 0.2 | 0.00077 | Axial |
| 2 | 30 | 0.0045 | 0.2 | 0.00069 | Axial |
| 3 | 35 | 0.0045 | 0.2 | 0.00080 | Center |
| 4 | 30 | 0.003 | 0.1 | 0.00058 | Factorial |
| 5 | 35 | 0.0045 | 0.2 | 0.00081 | Center |
| 6 | 30 | 0.006 | 0.3 | 0.00052 | Factorial |
| 7 | 35 | 0.003 | 0.2 | 0.00063 | Axial |
| 8 | 40 | 0.006 | 0.1 | 0.00097 | Factorial |
| 9 | 35 | 0.0045 | 0.2 | 0.00080 | Center |
| 10 | 35 | 0.0045 | 0.3 | 0.00077 | Axial |
| 11 | 35 | 0.0045 | 0.1 | 0.00088 | Axial |
| 12 | 35 | 0.0045 | 0.2 | 0.00086 | Center |
| 13 | 35 | 0.0045 | 0.2 | 0.00083 | Center |
| 14 | 35 | 0.0045 | 0.2 | 0.00084 | Center |
| 15 | 30 | 0.003 | 0.3 | 0.00044 | Factorial |
| 16 | 40 | 0.006 | 0.3 | 0.00091 | Factorial |
| 17 | 40 | 0.005 | 0.2 | 0.001 | Axial |
| 18 | 40 | 0.003 | 0.3 | 0.00072 | Factorial |
| 19 | 40 | 0.003 | 0.1 | 0.00083 | Factorial |
| 20 | 30 | 0.006 | 0.1 | 0.00069 | Factorial |

**Table 5.** Analysis of variance for the distillate production model.

| Response | Source | Sum of Squares | df | Mean Square | F-Value | *p*-Value | Remarks |
|---|---|---|---|---|---|---|---|
| Distillate | Model | $5.117 \times 10^6$ | 6 | $8.528 \times 10^5$ | 150.84 | <0.0001 | SD = 75.19<br>Mean = 2785<br>CV = 2.7<br>$R^2$ = 0.98<br>$R^2_{(adj)}$ = 0.97<br>$R^2_{(pred)}$ = 0.96<br>AP = 44.95 |
| | A: Feed-water temperature | $3.025 \times 10^6$ | 1 | $3.025 \times 10^6$ | 535.03 | <0.0001 | |
| | B: Flow rate | $5.760 \times 10^5$ | 1 | $5.760 \times 10^5$ | 101.88 | <0.0001 | |
| | C: Vacuum pressure | $4.410 \times 10^5$ | 1 | $4.410 \times 10^5$ | 78 | <0.0001 | |
| | AB | 31,250.00 | 1 | 31,250.00 | 5.53 | 0.0352 | |
| | AC | 31,250.00 | 1 | 31,250.00 | 5.53 | 0.0352 | |
| | $B^2$ | $6.264 \times 10^5$ | 1 | $6.264 \times 10^5$ | 108.56 | <0.0001 | |
| | Residual | 73,500 | 13 | 5653.85 | - | - | |
| | Lack of Fit | 40,166.67 | 8 | 5020.83 | 0.7531 | 0.6571 | |
| | Pure Error | 33,333.33 | 5 | 6666.67 | - | - | |

### *3.2. Effect of Independent Variables on Distillate Production*

A perturbation plot is typically used to examine the sensitivity of the factors (A, B, and C) to the response (distillate) in response surface methodology. The most significant factors are determined according to the most considerable changes in factors from low (−1) to high (1) levels. The perturbation plot between the inputs and the response is illustrated in Figure 5. The perturbation plot indicated that the two most significant factors contributing to the response were feed water temperature and flow rate. The response (distillate production) increased linearly with feed water temperature augmentation for the tested limits. In the case of flow rate, the distillate production increased with the flow rate up to a certain level, after which a drop in distillate collection was noticed. In the case of vacuum pressure, the distillate production decreased with an increment in vacuum pressure. From ANOVA, it was observed that the term BC is insignificant due to the high *p*-value. Hence, the combined effect of BC is not included in subsequent analysis and discussion.

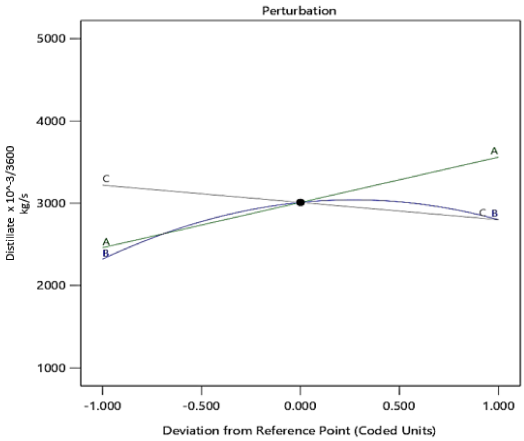


**Figure 5.** Perturbation plot between the inputs and response for specified limits.

The interaction and effect of independent variables, namely feed water temperature, flow rate, and vacuum pressure on distillate as the response is illustrated below in three-dimensional surface plots. The interaction between feed water temperature and flow rate is shown in Figure 6 and is found to be significant in distillate production. It is observed that an increase in feed water temperature increased distillate production. This is because for higher feed water temperatures, the fluid gets further heated in the boiler heat exchanger to greater temperatures before spraying into the flashing chamber. Higher feed water temperatures while spraying are always desirable as they lead to proper and effective fluid vaporization after spraying. These vapors move into the condenser to condense, ultimately increasing the distillate production. It can also be observed that as the feed water flow rate increased from 0.003 to 0.0045 kg/s, the distillate production also increased. However, a further increase in flow rate resulted in a decrease in output. This is due to the reason that for higher flow rates, the feed water travels quicker through the boiler heat exchanger, leading to a smaller temperature gradient across the boiler heat exchanger. This low temperature gradient impacts the spraying process and vaporization and leads to more brine collection compared to the distillate. This behavior is synchronous with the findings of Alrowais et al. [30], where the distillate production is found to increase up to a certain maximum with an increase in flow rate, after which there is some drop in the output.

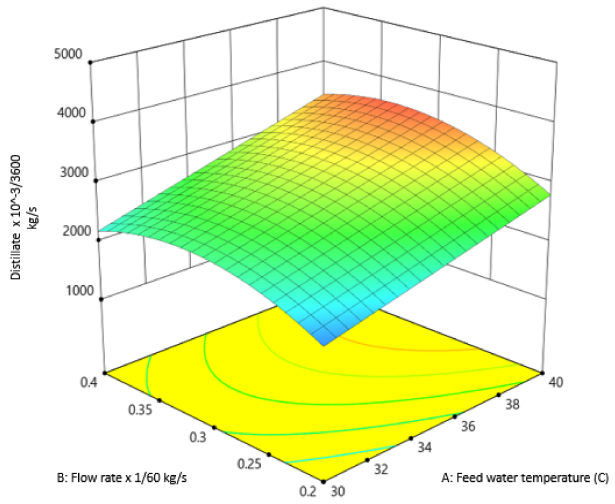


**Figure 6.** 3-D surface plot of the combined effect of feed water temperature and flow rate.

The interaction between feed water temperature and vacuum pressure is shown in Figure 7 and is significant for distillate production. It is observed that an increase in feed water temperature increased distillate production. However, an increase in vacuum

pressure resulted in a decrease in the output. This behavior is synchronous with Lovineh et al. [31], where the distillate production decreases with an increase in vacuum pressure.

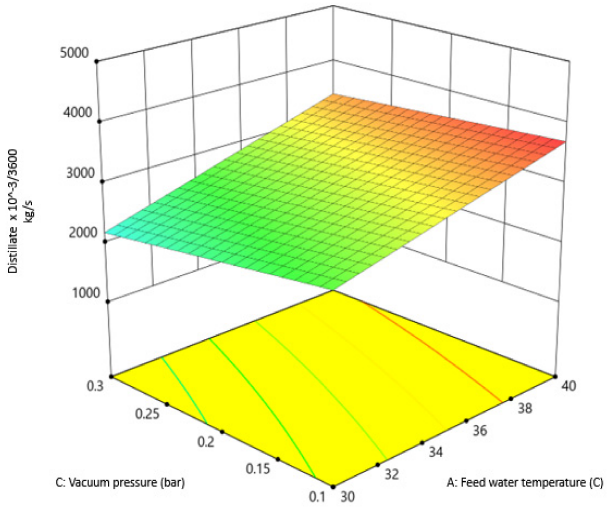


**Figure 7.** 3-D surface plot of the combined effect of feed water temperature and vacuum pressure.

Figure 8 shows the cube with distillate production at each factorial point. The cube plot indicates the reaction of feed water temperature (A), flow rate (B), and vacuum pressure (C) interact to affect the response. Because the model (Equation (2)) has the interaction term of AB and AC, the effects on the response are different when the variables are at their high levels. The diagnostic plot of the Box-Cox power transform is shown in Figure 9. The Box-Cox power transform is used to determine the requirement of model transformation. The curve's minimum point shows that the lambda value falls within 0 and 1, and no transformation was needed in the present condition. The diagnostic plot of actual versus predicted values of distillate production is illustrated in Figure 10. The points are closed to the diagonal line. It can be observed that there is a good fit between the experimental and model predicted values. This result also indicated that the model could predict well, and the predicted value is close to the actual value. The optimum experimental values and model predicted values are shown in Table 6. The maximum distillate production was predicted to be 0.00104 kg/s. Verification experiments were performed at the optimum values of process parameters, and the distillate production was found to be 0.00102 kg/s. The findings were in good agreement with the predicted values, indicating the developed model's accuracy.

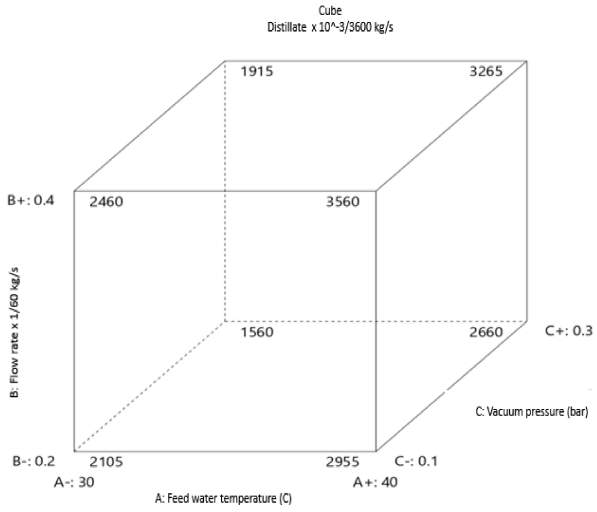


**Figure 8.** Cube plot of distillate production at each factorial point.

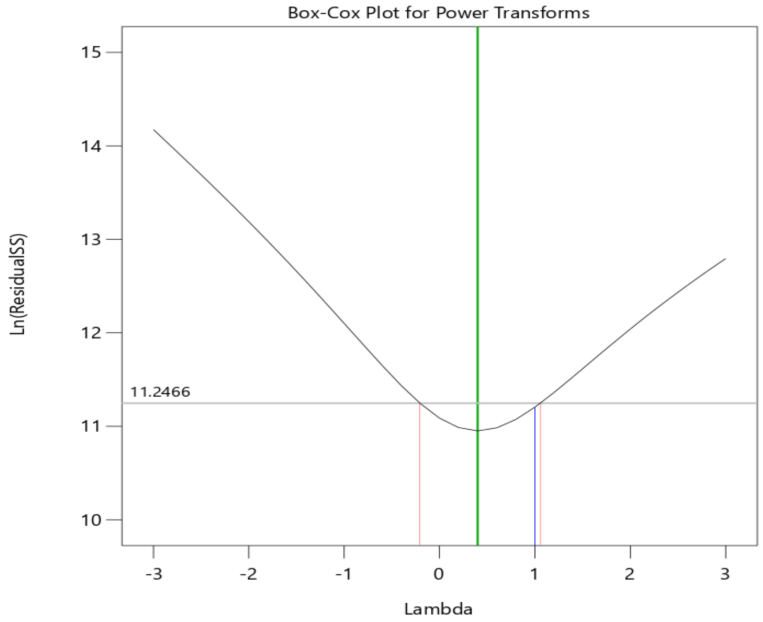


**Figure 9.** The diagnostic plot of Box-Cox for power transforms.

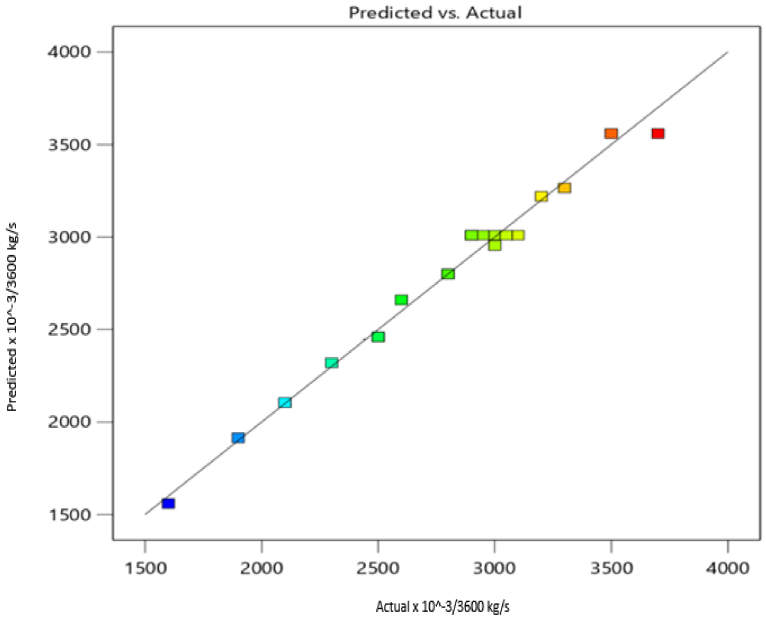


**Figure 10.** The diagnostic plot of actual versus predicted values for distillate production.

**Table 6.** Optimum experimental and model predicted values of distillate production.

| Feed-Water Temperature (°C) | Flow Rate (kg/s) | Vacuum Pressure (Bar) | Distillate Production (kg/s × $10^{-3}$/3600) | | Desirability | Error % |
|---|---|---|---|---|---|---|
| | | | Experimental | Predicted | | |
| 40 | 0.005 | 0.1 | 3700 | 3758 | 0.95 | 1.5 |

## 4. Energy and Exergy Analysis

For analyzing the performance of a system, modelling is done by means of carrying out energy and exergy analysis. The energy and exergy analysis of the concentrator plate heat exchanger is done for the optimal conditions and illustrated in the following sub-sections.

### *4.1. Energy Analysis*

Some general assumptions are made in this analysis, considering steady flow conditions, the reflector and concentrator plate surfaces to be free of dirt, and clear weather conditions.

The amount of heat absorbed by the feed water across the concentrator plate heat exchanger can be computed from the general Equation:

$$Q_{ab} = mC_p(T_o - T_i) \quad (3)$$

where:
$m$ is mass flow rate, kg/s$C_p$ is specific heat, J/kg K
$T_o$ is fluid exit temperature, K
$T_i$ is fluid inlet temperature, K

The amount of solar radiation incident on the concentrator plate heat exchanger can be written as described by Malik et al. [32]:

$$Q_i = I_t A \quad (4)$$

where:
$Qi$ is the amount of heat incident on concentrator plate heat exchanger, W
$I_t$ is the total solar intensity incident on the heat exchanger, W/m$^2$
$A$ is the effective surface area of concentrator plate heat exchanger, m$^2$

There will also be some heat loss taking place from the surface of the concentrator plate heat exchanger to the surroundings resulting from the temperature difference between the heat exchanger surface and surroundings. This heat loss is computed as:

$$Q_L = U_L A(T_c - T_a) \quad (5)$$

where:
$Q_L$ is heat loss from heat exchanger surface to surroundings, W
$U_L$ is the overall loss coefficient for heat exchanger, W/m$^2$·K
$T_c$ is the average temperature of heat exchange surface, K
$T_a$ is ambient air temperature, K

The net heat absorbed that is available on the concentrator plate heat exchanger is calculated as the difference between the incident heat and the heat loss to the surroundings.

$$Q_{net} = I_t A - U_L A(T_c - T_a) \quad (6)$$

where:
$Q_{net}$ is the net heat input on the concentrator plate heat exchanger, W

The energy efficiency of the concentrator plate heat exchanger (EN-CPHE) is the ratio of useful energy to the total energy.

$$\eta_{EN-CPHE} = \frac{Q_{ab}}{Q_{net}} \quad (7)$$

### *4.2. Exergy Analysis of Concentrator Plate Heat Exchanger*

Exergy is destroyed as the solar energy is converted to thermal energy inside the concentrator plate heat exchanger. The exergy is computed as described by Gomri [33].

$$\text{Exergy destroyed} = \text{Total exergy} - \text{exergy transferred to the fluid}$$

$$\dot{X_{des}} = \dot{X_T} - \dot{X_U} \quad (8)$$

$$\dot{X_{des}} = IA\left(1 - \frac{T_e}{T_s}\right) - \eta_{EN-CPHE}Q_{ab}\left(1 - \frac{T_e}{T_{fm}}\right) \quad (9)$$

where:
$T_e$ is environment temperature, K
$T_s$ is sun temperature, 5800 K
$T_{fm}$ is the mean fluid temperature for the heat exchanger

The exergy efficiency of the concentrator plate heat exchanger (EX-CPHE) is the ratio of useful exergy to total exergy.

$$\eta_{EX-CPHE} = \frac{\dot{X}_U}{\dot{X}_T} \quad (10)$$

From the above analysis, the energy efficiency was found to be 58%, and the exergy efficiency was 1.03%. A similar analysis is reported in the work of Sutanto et al. [34] and Mirmanto et al. [35], which are referred while carrying out this analysis.

## 5. Conclusions

In the present study, experiments were performed to obtain distilled water using the coastal seawater of Al-Khobar city in Saudi Arabia as a feed water source. The effect of three process parameters, namely feed water temperature, flow rate, and vacuum pressure, was studied. Additionally, RSM was applied to determine the optimum feed water temperature, flow rate, and vacuum pressure values for maximizing the response. The system exhibited optimum performance at a feed water temperature of 40 °C, a flow rate of 0.005 kg/s, and a vacuum pressure of 0.1 bar. For these conditions, an optimum distillate production of 0.001 kg/s was achieved. The developed distillate model predicted the system performance reasonably well, with an error of less than 5%. The current findings help the researcher identify the most significant factor and optimize distillate production.

**Author Contributions:** F.A. and M.S.A.A. wrote the original draft of the manuscript; M.R.R.M.A.Z., K.C.Y., F.S., D.S.C.H., M.A.A.M.S. and M.K. edited the manuscript, data curation, validation, and prepared the technical aspects of the paper. All authors have read and agreed to the published version of the manuscript.

**Funding:** This research was funded by the Ministry of Higher Education Malaysia under Fundamental Research Grant Scheme with Project Code FRGS/1/2021/TK0/USM/02/17.

**Institutional Review Board Statement:** Not applicable.

**Informed Consent Statement:** Informed consent was obtained from all subjects in the study.

**Data Availability Statement:** The data presented in this study are available on request from the corresponding author.

**Acknowledgments:** Acknowledgement to School of Mechanical Engineering, Universiti Sains Malaysia.

**Conflicts of Interest:** The authors declare no conflict of interest.

## References

1. Risse, B.; Spitzer, D.; Hassler, D.; Schnell, F.; Comet, M.; Pichot, V.; Muhr, H. Continuous formation of submicron energetic particles by the flash-evaporation technique. *Chem. Eng. J.* **2012**, *203*, 158–165. [CrossRef]
2. Lv, H.; Wang, Y.; Wu, L.; Hu, Y. Numerical simulation and optimization of the flash chamber for multi-stage flash seawater desalination. *Desalination* **2019**, *465*, 69–78. [CrossRef]
3. Cheng, W.; Zhang, W.; Cheng, H.; Hu, L. Spray cooling and flash evaporation cooling: The current development and application. *Renew. Sustain. Energy Rev.* **2016**, *55*, 614–628. [CrossRef]
4. Gandhidasan, P. Quick performance prediction of liquid desiccant regeneration in a packed bed. *Sol. Energy* **2005**, *79*, 47–55. [CrossRef]
5. Ezzat, A.W.; Hu, E.; Al-Najjar, H.M.T.; Zhao, Z.; Shu, X. Investigation of steam jet flash evaporation with solar thermal collectors in water desalination systems. *Therm. Sci. Eng. Prog.* **2020**, *20*, 100710. [CrossRef]
6. Chen, L.X.; Hu, P.; Sheng, C.C.; Zhang, N.; Na Xie, M.; Wang, F.X. Thermodynamic analysis of three ejector based organic flash cycles for low grade waste heat recovery. *Energy Convers. Manag.* **2019**, *185*, 384–395. [CrossRef]
7. Lin, S.; Zhao, H.; Zhu, L.; He, T.; Chen, S.; Gao, C.; Zhang, L. Seawater desalination technology and engineering in China: A review. *Desalination* **2021**, *498*, 114728. [CrossRef]

8. Miyatake, O.; Koito, Y.; Tagawa, K.; Maruta, Y. Transient characteristics and performance of a novel desalination system based on heat storage and spray flashing. *Desalination* **2001**, *137*, 157–166. [CrossRef]
9. Lai, X.; Long, R.; Liu, Z.; Liu, W. Solar energy powered high-recovery reverse osmosis for synchronous seawater desalination and energy storage. *Energy Convers. Manag.* **2021**, *228*, 113665. [CrossRef]
10. Ghorbani, B.; Mehrpooya, M.; Dadak, A. Thermo-economic analysis of a solar-driven multi-stage desalination unit equipped with a phase change material storage system to provide heating and fresh water for a residential complex. *J. Energy Storage* **2020**, *30*, 101555. [CrossRef]
11. Gao, W.; Qi, J.; Zhang, J.; Chen, G.; Wu, D. An experimental study on explosive boiling of superheated droplets in vacuum spray flash evaporation. *Int. J. Heat Mass Transf.* **2019**, *144*, 118552. [CrossRef]
12. Ji, C.; Cheng, L.; Wang, N.; Liu, Z. Experimental investigation on high-pressure high-temperature spray flash evaporation and the characteristic Jakob number. *Exp. Therm. Fluid Sci.* **2019**, *102*, 94–100. [CrossRef]
13. Muthunayagam, A.; Ramamurthi, K.; Paden, J. Low temperature flash vaporization for desalination. *Desalination* **2005**, *180*, 25–32. [CrossRef]
14. Ikegami, Y.; Sasaki, H.; Gouda, T.; Uehara, H. Experimental study on a spray flash desalination (influence of the direction of injection). *Desalination* **2006**, *194*, 81–89. [CrossRef]
15. Fathinia, F.; Al-Abdeli, Y.M.; Khiadani, M. Evaporation rates and temperature distributions in fine droplet flash evaporation sprays. *Int. J. Therm. Sci.* **2019**, *145*, 106037. [CrossRef]
16. Peng, Y.; Cheng, W. Experimental investigation on the effect of heat transfer enhancement of vacuum spray flash evaporation cooling using $Al_2O_3$–water nanofluid. *Energy Procedia* **2017**, *142*, 3766–3773. [CrossRef]
17. Guo, Y.; Ma, H.; Fu, B.; Ji, Y.; Su, F.; Wilson, C. Heat Transfer Analysis of Flash Evaporation with MEPCM. *J. Thermal Sci. Eng. Appl.* **2019**, *11*, 051016. [CrossRef]
18. Jurkowska, M.; Szczygieł, I. Review on properties of microencapsulated phase change materials slurries (mPCMS). *Appl. Therm. Eng.* **2016**, *98*, 365–373. [CrossRef]
19. Ali, S.; Mustafa, M. Barriers facing Micro-encapsulated Phase Change Materials Slurry (MPCMS) in Photovoltaic Thermal (PV/T) application. *Energy Rep.* **2020**, *6*, 565–570. [CrossRef]
20. Yu, Q.; Romagnoli, A.; Yang, R.; Xie, D.; Liu, C.; Ding, Y.; Li, Y. Numerical study on energy and exergy performances of a microencapsulated phase change material slurry based photovoltaic/thermal module. *Energy Convers. Manag.* **2019**, *183*, 708–720. [CrossRef]
21. Chen, Q.; Xu, G.; Xia, P. The performance of a solar-driven spray flash evaporation desalination system enhanced by microencapsulated phase change material. *Case Stud. Therm. Eng.* **2021**, *27*, 101267. [CrossRef]
22. Moharram, N.A.; Bayoumi, S.; Hanafy, A.A.; El-Maghlany, W.M. Hybrid desalination and power generation plant utilizing multi-stage flash and reverse osmosis driven by parabolic trough collectors. *Case Stud. Therm. Eng.* **2021**, *23*, 100807. [CrossRef]
23. Gnaifaid, H.; Ozcan, H. Multi-objective optimization of a concentrated solar energy driven trigeneration plant with thermal energy storage: A case study for Turkey. *Case Stud. Therm. Eng.* **2020**, *20*, 100642. [CrossRef]
24. Aziz, M.A.; Abdullah, M.; Khor, C.; Azid, I. Optimization of pin through hole connector in thermal fluid–structure interaction analysis of wave soldering process using response surface methodology. *Simul. Model. Pract. Theory* **2015**, *57*, 45–57. [CrossRef]
25. Ishak, M.H.H.; Ismail, F.; Aziz, M.S.A.; Abdullah, M.Z.; Abas, A. Optimization of 3D IC stacking chip on molded encapsulation process: A response surface methodology approach. *Int. J. Adv. Manuf. Technol.* **2019**, *103*, 1139–1153. [CrossRef]
26. Lim, C.H.; Abdullah, M.Z.; Aziz, I.A.; Khor, C.Y.; Aziz, M.S.A. Optimization of flexible printed circuit board's cooling with air flow and thermal effects using response surface methodology. *Microelectron. Int.* **2021**, *38*, 182–205. [CrossRef]
27. Joy, V.M.; Feroz, S.; Dutta, S. Solar nanophotocatalytic pretreatment of seawater: Process optimization and performance evaluation using response surface methodology and genetic algorithm. *Appl. Water Sci.* **2021**, *11*, 18. [CrossRef]
28. Salih, F.Y.M.; Sakhile, K.; Shaik, F.; Lakkimsetty, N.R. Treatment of petroleum wastewater using synthesised haematite ($\alpha$-$Fe_2O_3$) photocatalyst and optimisation with response surface methodology. *Int. J. Environ. Anal. Chem.* **2020**, 1–20. [CrossRef]
29. Mohammadi, T.; Safavi, M. Application of Taguchi method in optimization of desalination by vacuum membrane distillation. *Desalination* **2009**, *249*, 83–89. [CrossRef]
30. Alrowais, R.; Qian, C.; Burhan, M.; Ybyraiymkul, D.; Shahzad, M.W.; Ng, K.C. A greener seawater desalination method by direct-contact spray evaporation and condensation (DCSEC): Experiments. *Appl. Therm. Eng.* **2020**, *179*, 115629. [CrossRef]
31. Lovineh, S.; Asghari, M.; Rajaei, B. Numerical simulation and theoretical study on simultaneous effects of operating parameters in vacuum membrane distillation. *Desalination* **2013**, *314*, 59–66. [CrossRef]
32. Malik, A.; Qureshi, S.R.; Abbas, N.; Zaidi, A.A. Energy and exergy analyses of a solar desalination plant for Karachi Pakistan. *Sustain. Energy Technol. Assessments* **2020**, *37*, 100596. [CrossRef]
33. Gomri, R. Energy and exergy analyses of seawater desalination system integrated in a solar heat transformer. *Desalination* **2009**, *249*, 188–196. [CrossRef]

34. Bayu, S.; Yuli, S.I.; Agung, T.W.; Hector, I. Enhancing the performance of floating photo-voltaic system by using thermosiphon cooling method: Numerical and experimental analyses. *Int. J. Therm. Sci.* **2022**, *180*, 107727.
35. Mirmanto; Sayoga, I.M.A.; Wijayanta, A.T.; Sasmito, A.P.; Aziz, M. Enhancement of Continuous-Feed Low-Cost Solar Distiller: Effects of Various Fin Designs. *Energy* **2021**, *14*, 4844. [CrossRef]